Geochemistry Geophysics Geosystems G3
AN ELECTRONIC JOURNAL OF THE EARTH SCIENCES
Published by AGU and the Geochemical Society

Article
Volume 5, Number 12
30 December 2004
Q12015, doi:10.1029/2004GC000771
ISSN: 1525-2027

Decoding nonlinear growth rates in biogenic environmental archives

Fjo De Ridder, Rik Pintelon, and Johan Schoukens
Department of Electricity and Instrumentation, Team B: System Identification, Vrije Universiteit Brussel, Pleinlaan 2, B-1050 Brussels, Belgium (federid@pop.vub.ac.be)

David Paul Gillikin
Analytical and Environmental Chemistry Department, Vrije Universiteit Brussel, Pleinlaan 2, B-1050 Brussels, Belgium

Luc André
Section of Petrography-Mineralogy-Geochemistry, Royal Museum for Central Africa, B-3080 Tervuren, Belgium (lucandre@africamuseum.be)

Willy Baeyens, Anouk de Brauwere, and Frank Dehairs
Analytical and Environmental Chemistry Department, Vrije Universiteit Brussel, Pleinlaan 2, B-1050 Brussels, Belgium (fdehairs@vub.ac.be)

[1] The record of an environmental proxy along a growth axis in biogenic carbonates can reflect changing environmental conditions experienced during the lifetime of the organism. When a chronology of the growth axis is not available, a method based on anchor points is commonly used to introduce a time grid. Between these anchor points a constant growth rate is generally assumed, despite the fact that growth rates change during life in most organisms. Here, we present a method which refines the constant growth rate assumption, at least in situations where the environmental proxy has a periodic component in its signal. A nonlinear growth rate can then be estimated, enabling the construction of a more realistic time base. The anchor point method and the method proposed here are first compared on a synthetic record. It is shown that the choice of the anchor points, which is always a subjective one, is largely influenced by the stochastic noise on the data record. This results in biased growth rate profiles and biased time grids. Next we apply the method on the Mg record in the bivalve *Isognomon ephippium*, on three samples of the clam *Saxidomus giganteus* from Washington State and on the Vanuatu coral stable isotope record. The method developed is applicable to a wide range of proxy records, which are measured along an indirect time grid and are complicated by nonlinear accretion rates. Furthermore, this method which takes variable growth rates into account opens perspectives on quantitative modeling of the relationship between environmental proxies recorded by accretive archives and the instrumental record, like temperature or salinity.

Components: 7456 words, 14 figures, 2 tables.

Keywords: growth and accretion rate; time base distortion; stable isotopes; carbonate; environmental proxies; paleoclimate.

Index Terms: 3210 Mathematical Geophysics: Modeling; 4870 Oceanography: Biological and Chemical: Stable isotopes; 4875 Oceanography: Biological and Chemical: Trace elements.

Received 10 June 2004; **Revised** 2 September 2004; **Accepted** 19 October 2004; **Published** 30 December 2004.

De Ridder, F., R. Pintelon, J. Schoukens, D. P. Gillikin, L. André, W. Baeyens, A. de Brauwere, and F. Dehairs (2004), Decoding nonlinear growth rates in biogenic environmental archives, *Geochem. Geophys. Geosyst.*, *5*, Q12015, doi:10.1029/2004GC000771.

1. Introduction

[2] Earth's climate system varies on a range of time scales due to natural and anthropogenic forcings. Predictions of future climate requires that global climate models are tested and validated against instrumental measurements of meteorological and environmental data, and also against long-term records of paleoclimate based on trace element and isotopic records preserved in layered substrates. Such climate and environmental information can be traced back from proxy records in many solid substrates characterized by a wide range of accretion rates, e.g., sclerosponges [*Lazareth et al.*, 2000], speleothems [*Verheyden et al.*, 2000; *Finch et al.*, 2001], corals [*Marshall and McCulloch*, 2002; *Wei et al.*, 2000; *Kuhnert et al.*, 2002; *Fallon et al.*, 1999; *Sinclair et al.*, 1998], bivalves [*Lazareth et al.*, 2003; *Vander Putten et al.*, 1999, 2000], sediments [*Weedon*, 1989; *Herbert*, 1994; *Martinson et al.*, 1987] and ice cores [*Petit et al.*, 1999].

[3] In such data series, the environmental proxy is not measured directly as a function of time, but along a growth or accretion axis. Since we are mostly interested in the time series this distance profile has to be transformed into a time profile (Figure 1), which requires knowledge about growth or accretion rate. In general, it is not possible to estimate the growth or accretion rate and the time profile from the distance grid. So, without extra information or extra assumptions, one has to date at least two observations and assume a constant growth rate to construct a time series. This is illustrated by the dotted line in Figure 1. An example of such extra information are growth bands, present in some corals, bivalves or trees, which can be used to date the record, employing, e.g., the anchor point method [*Jones*, 1983; *Paillard et al.*, 1996]. However, this can introduce non-negligible bias, as will be shown in a simulation (section 3). Furthermore, even when growth lines are available, they usually only provide information about variations on annual and multiannual scales and not on a subannual scale.

[4] In the present paper, we propose a method to transform the distance scale into a time scale, based on the periodicity of the record and allowing for the reconstruction of growth rate and time series. Fluctuations in growth rate are reconstructed by demodulating the side peaks in the Fourier spectrum, which are sometimes incorrect interpreted as noise. The variations in growth rate are modeled as a distortion of the time base. Once the distortion is known, a more accurate time base can be reconstructed eventually resolving interannual variation.

[5] First, we compared the underlying assumptions of the method with those of the anchor point method [*Jones*, 1983; *Paillard et al.*, 1996]. Next, both methods are tested and validated using simulation data. Finally, some applications are discussed: (1) the Mg record in the bivalve *Isognomon epphippium* (Tudor Creek, Mombasa, Kenya); (2) the $\delta^{18}O$ records of three specimen of the bivalves *Saxidomus giganteus* (Washington, U.S.A.); and (3) a Vanuatu coral stable isotope data. The method developed is applicable to a large range of accretive substrates which are measured along a distance grid and have to be transformed into time series.

2. Conceptual Approach of the Time Base Distortion Method

[6] Usually the conversion from a spatial scale to a time scale assumes a stepwise constant growth rate. In the following sections, we first describe how variations in growth rate can be expressed as a distortion of linear growth rate, followed by a method to estimate this distortion of the time base.

2.1. A Model for the Time Base Distortion

[7] The growth rate is not estimated directly. On the one hand we know the distances between subsequent observations and on the other hand we would like to know the time instances between these observations. The ratio of both is the growth rate. To estimate the time instances, we start from an average constant growth rate, where the time instances between the observations are constant. So the time instance at which the nth observation was formed is given by

$$t_n = nT_s. \tag{1}$$

In equation (1), T_s is the sample period (dimension is time), which is a measure for the average time instance between two subsequent observations. This constant growth rate model would correspond to the dotted line on the diagonal of Figure 1. Equation (1) will not be valid when the time instances are disturbed, due to variations in growth or accretion rate. This distortion of the time base can be modeled by a distortion term, $g(n)$, which is (1) zero when the growth is equal to the average

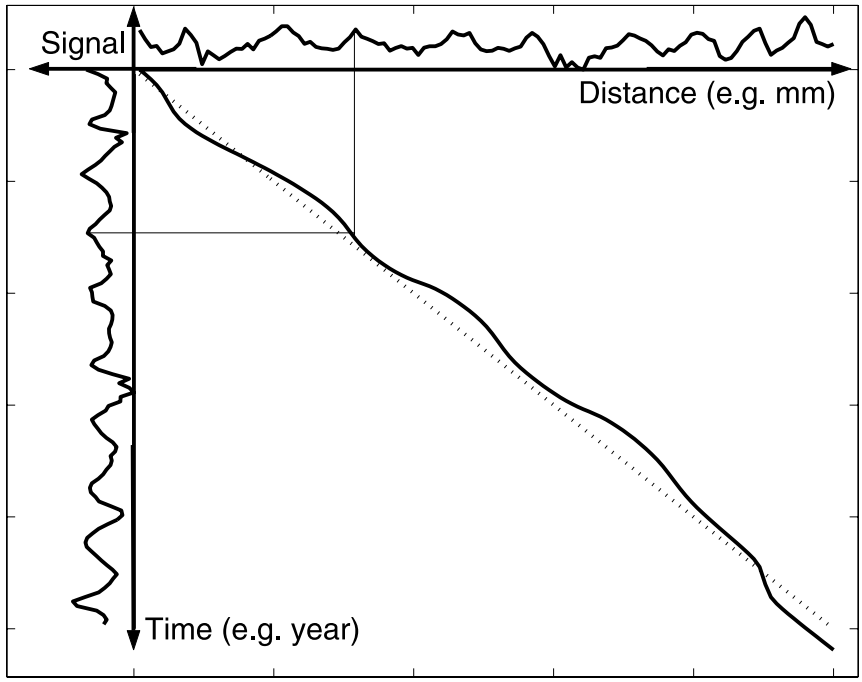

Figure 1. Conceptual graph showing the transformation from a record along a distance grid to time series. The dotted line represents a constant growth rate, while the curved line along the diagonal represents the real growth rate (data of Clam 2 are used, which is discussed in section 5).

growth, (2) negative when the growth is slower than the average and (3) positive when the growth is greater than the average. So, an improved estimate of the time instant at which observation n was formed is given by

$$t_n = nT_s + g(n)T_s, \tag{2}$$

where the first term expresses the constant time step and $g(n)$ will be called the time base distortion (TBD) at observation position n (scalar quantity). The TBD is the difference between the dotted and the full line on the diagonal of Figure 1. Note that at this stage no assumptions are made about the TBD: any possible variation in the growth can be expressed by equation (2). In the next section we explain how the TBD can be estimated.

2.2. Identification of the Time Base Distortion

[8] In order to estimate the TBD, $g(n)$, we have to add an additional assumption since the data alone carry not enough information to determine the TBD uniquely. Many possibilities exist. In this paper we assume that the sampled signal is periodic, i.e., if the observations are modeled by a sum of sines and cosines, no systematic error is made. Periodic records can most easily be interpreted in a Fourier spectrum. Figure 2a shows a sinusoidal signal as function of time. The corresponding Fourier spectrum is shown in Figure 2b: one peak appears at a frequency of one year^{-1}. If a TBD is introduced, e.g., due to variations in growth rate, the measured record could look like Figure 2c. If a constant growth rate of one mm/year is used to construct a time base, the spectral interpretation becomes much more complicated (Figure 2d): small side peaks appear symmetrically around a broadened central peak. How these side peaks and broadened central peak can be decoded to reconstruct the TBD and accretion rate is elaborated in the present paper. The mathematical details of the procedure are given in Appendix A and also by *Verspecht* [1994] and *Schoukens et al.* [1997]. The method has some important limitations that need to be detailed before we can interpret the results: the time base is separated by isolating a window around the first harmonic in the spectrum. The larger this window is, the more detailed the TBD will be. However, with an increasing window width the influence of the stochastic noise on the TBD will increase as

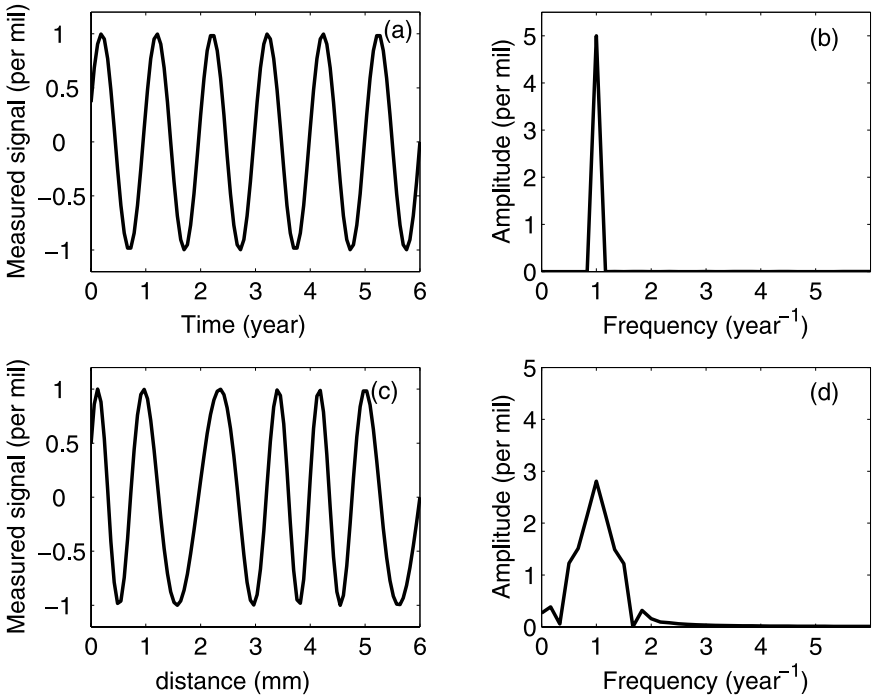

Figure 2. Deformation of the Fourier spectrum, due to variations in accretion rate: (a) sinusoidal signal as function of time, (b) its spectrum, (c) the measured signal as a function of the distance, and (d) its spectrum assuming a constant accretion rate of one (mm/year). Notice that the TBD is coded around the harmonic and in its side peaks.

well. If the width of the selected window is too large, such that side peaks of the second harmonic are included, these will be misinterpreted as a distortion of the first harmonic.

3. Comparison With the Anchor Point Method

[9] The anchor point method assumes that the date of some observations is known. This method, used to construct a time base is used for more than twenty years, e.g., [*Jones*, 1983]. A software package for this method is provided by *Paillard et al.* [1996]. Next, the time instances of the observations in between these observations can be estimated by assuming a stepwise constant accretion rate. This anchor point method is based on three assumptions which are compared with the assumptions made by the TBD (see also Table 1). Next, a synthetic record is simulated in order to test and compare both methods.

3.1. Comparison of the Assumptions

3.1.1. First Assumption

[10] In the case of nonperiodic records, the TBD method cannot be used. Therefore we will focus on detailed data records with subannual variations. In this situation, the anchor-point method makes one additional assumption for each additional year, i.e., the user has to define the timing of a periodic event in the record. Selecting these events is much more sensitive to noise than assuming a periodic record (see section 3.2). The user has not only to decide on the timing of each event, but also the number of events. In noisy records, events can easily be overlooked or a particular year can be incorrectly represented as

Table 1. Comparison of the Underlying Assumptions Made by the TBD and by the Anchor Point Method

	TBD	Anchor Point
1	Record has a periodic component.	The number of anchor points is known and each one is dated.
2	Two arbitrary observations are dated.	First and last observation are dated.
3	TBD is bandwidth limited.	Within two anchor points the growth rate is constant.

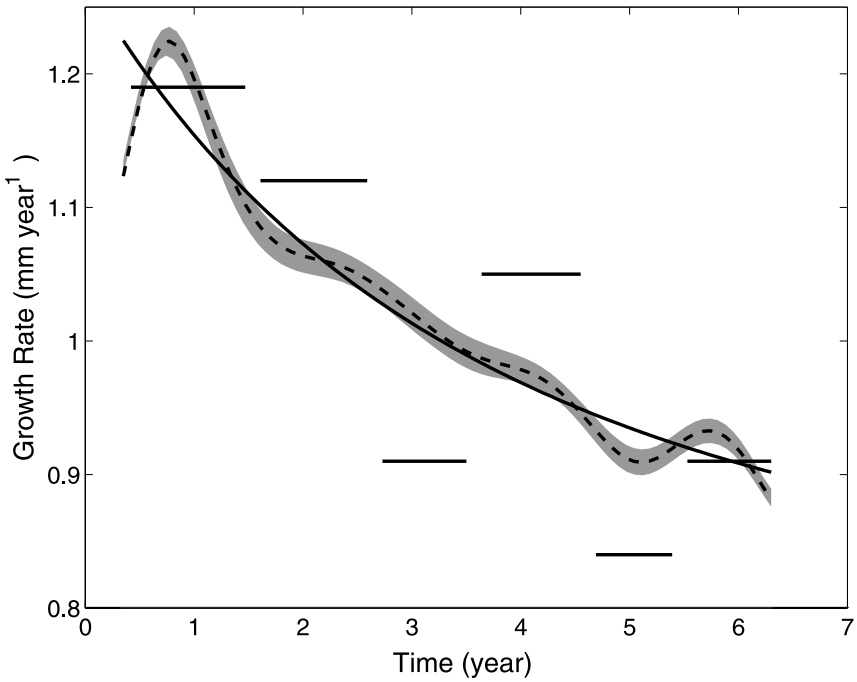

Figure 3. Simulated (full line) and reconstructed growth rates (dashed line: TBD method and horizontal line: anchor point method). Simulated (full line) and reconstructed growth rates (dashed line: TBD method and horizontal line: anchor point method). The gray area represents the 95% uncertainty bound estimated with a Monte Carlo simulation of 100 runs.

two years. The latter problem becomes particularly acute when the record consists of multiple harmonics, which is often the case in tropical regions because of possible effects due to bimodal temperature and rainfall patterns.

3.1.2. Second Assumption

[11] The TBD method cannot assess the time span of a period. To translate this information into a time scale at least two events have to be dated. The anchor-point method dates all events in between the first and last anchor point. Observations which are not in between the first and last anchor point cannot be dated.

3.1.3. Third Assumption

[12] Due to the size of the window, used to separate the TBD, this TBD will be bandwidth limited. This means that high frequency variations in the TBD fall outside this window and will cause an error in the predicted growth rate. Another disadvantage is that the width of the window and thus the bandwidth of the TBD is chosen by the user and thus subjective. On the other hand, the anchor point method assumes a constant growth rate within two anchor points. Consequently, hiatuses or any other variation in growth rate between the selected anchor points will introduce an error.

3.2. Comparison of Both Methods Based on a Simulation

[13] The anchor point and TBD methods are compared using a synthetic data record consisting of 100 observations of a sinusoid with amplitude one and frequency one year^{-1}, the sample period is T_s = 0.07 year, so that exactly seven years are recorded. The time grid is distorted so as to mimic a growth rate that slows down exponentially. The TBD was in this case $g(n) = 3.18 - 2.98t + 0.55t^2 - 0.02t^3$, with $t = nT_s$. The record is disturbed by Gaussian noise, such that the signal-to-noise ratio equals ten. (The signal-to-noise ratio is the ratio of the root-mean-square value of the noise free model by the root-mean-square value of the particular noise realization.) We have selected the maximum in each period as an annual anchor point. The window width, used to isolate the time base distortion, covered the spectral content in the region from $1 - 0.28 = 0.72$ year^{-1} to $1 + 0.28 = 1.28$ year^{-1}. The growth rate results obtained by both methods are compared with the actual synthetic growth rate (Figure 3). The first and last half

year are excluded because the anchor point method cannot give growth rate information in these regions and the growth rates predicted by the TBD method are unreliable because of ringing [*Schoukens et al.*, 1997]. Both reconstructed growth rates more or less follow an exponential decrease, although the TBD method provides a better match to the simulated growth rate. The root-mean-square values of the difference between the calculated and simulated growth rates are 70 μm year^{-1} for the anchor point method and 20 μm year^{-1} for the TBD method. The gray bound on Figure 3 is the 95% uncertainty bound estimated with a Monte Carlo simulation of one hundred runs. This bound shows that the TBD method is relatively insensitive to stochastic noise variations. However, systematic errors, due to the limited bandwidth and ringing are reproduced in each run of the simulation and are thus not detected by the Monte Carlo simulation. The first systematic error can be seen in the wiggles of the reconstructed growth rate and the second at the edges. We have chosen this simulation to illustrate that even under optimal conditions (signal-to-noise-ratio of ten) the anchor point method can produce unreliable results. The reason for this is that the user has to decide which events are selected as anchor points. The noise on the measurements has a large influence on the selection of a particular event (e.g., a maximum or minimum in the record). Selecting the wrong event as anchor point will largely influence the growth rate. Consequently, a bias the time grid of the preceding and following period is introduced. The TBD method on the contrary bears on all observations, and hence the noise on a particular event will have a much smaller influence on the result.

4. Case Study 1: The Bivalve *Isognomon ephippium*

[14] In this first example the TBD method is discussed in detail, to clarify the range of applications, benefits and shortcomings. First, the record is analyzed while assuming a constant growth rate. This way, the largest extremes in the spectrum can already be interpreted and the spectral contents, which carry information about growth rate, can be shown. Next, results obtained via the TBD method and the anchor point method are compared. It is well known from literature that sea surface temperature is a major external control on Mg incorporation in calcite [*Klein et al.*, 1996; *Lazareth et al.*, 2003], and we will use the correlation between SST and the Mg signal as a validation of the deduced time base.

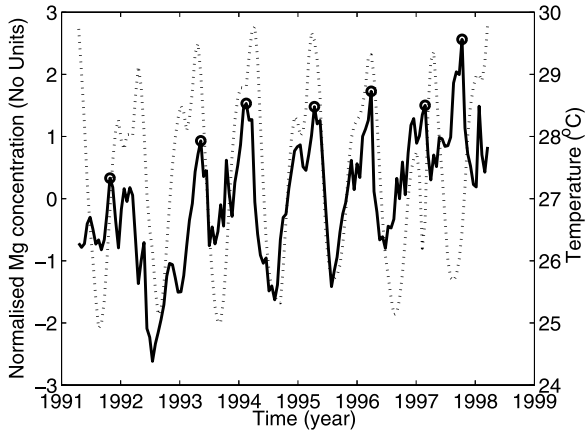

Figure 4. Mg signal measured along the growth axis in an *Isognomon ephippium* (full line) versus instrumental SST (dotted line), assuming a constant growth rate (correlation coefficient R = 0.37). The "o" indicates annual maxima that we have chosen to test the anchor point method.

4.1. Data Record

[15] The *I. ephippium* specimen was collected in August 1998 from Tudor Creek, nearby the city of Mombasa, Kenya. A more detailed description of the measurements and a discussion of other trace elements, as well as the analysis of other specimens of this species, are given by *Lazareth et al.* [2003]. Monthly averaged values of sea surface temperature (SST) were obtained from the Web site http://ingrid.ldgo.columbia.edu/SOURCES/.IGOSS/.nmc/.monthly/.sst as blended from ship, buoy and bias-corrected satellite data.

[16] High-resolution spatial sampling of the calcite layer was performed with a Laser Ablation Inductively Coupled Plasma-Mass Spectrometer system from the umbo toward the growing tip (one laser shot approximately every 230 μm with a diameter of 60 μm). In this way, successively formed layers were sampled. Ca was used as internal standard and the Mg signals were normalized (subtraction of the mean and divided by the standard deviation).

4.2. A Constant Growth Rate

[17] Assuming the minima and maxima of the Mg signal in *I. ephippium* reflect seasonal temperature periodicity, an average growth rate of 4.8 mm year^{-1} (seven maxima over a distance of 33.5 mm) was calculated. The Mg signal and the

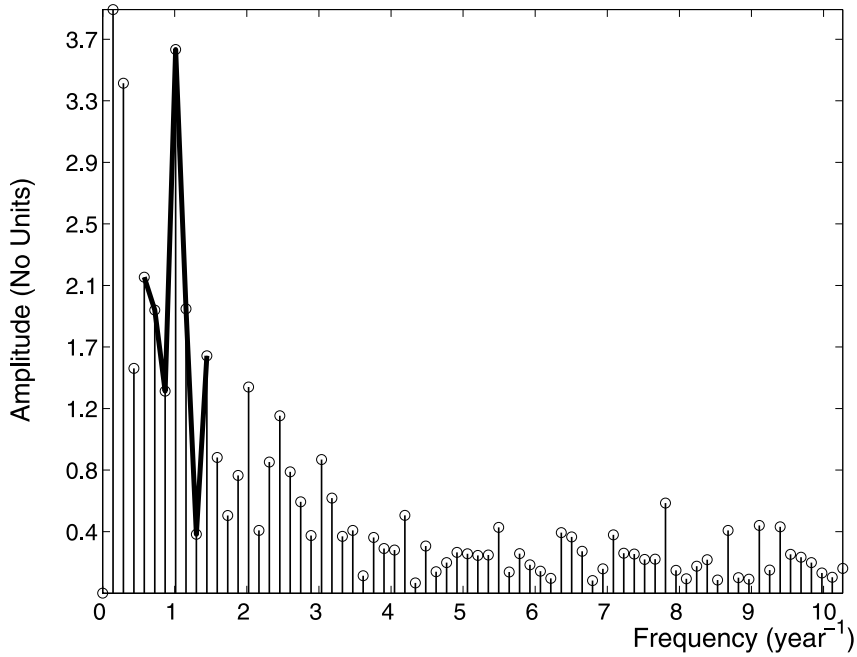

Figure 5. Discrete Fourier spectrum of the Mg signal in *I. ephippium*. The window is represented by the full line, which covers the spectral contents from 0.57 year^{-1} to 1.57 year^{-1}.

temperature record are shown in Figure 4. However, we noticed the occurrence of a second smaller Mg peak just before the annual Mg maxima (Figure 4), which can also be noticed in the SST profiles. Despite these similarities, three peculiarities must be pointed out: (1) although the smaller peaks are too regular to reflect stochastic noise, the peak correspondence between Mg signal and SST is rather poor (Figure 4); (2) the Mg concentration increases along the growth axis, suggesting some physiological control on Mg incorporation (e.g., growth rate); (3) from the observed deviation the distance between successive maxima in the Mg profile with those in the SST profile, it is clear that bivalve growth differed from year to year.

[18] Assuming a constant growth rate, the correlation coefficient between Mg and SST is rather weak ($R = 0.37$ ($n = 145$, $p < 0.01$)); some peaks coincide, but others are shifted along the time axis). During the cooler seasons of 1993 and of 1997 the Mg signal decreases, as it does in the other years, but the minimum does not reach as low. A possible explanation is that the specimen stopped growing during particular events and corresponding sequences of the proxy record are missing. Such offsets are responsible for the poor correlation observed.

[19] To summarize, the assumption of a constant growth rate is inadequate to predict relations on an interannual scale (even annual variations suffer from variability in growth rate).

4.3. Nonlinear Growth

[20] The largest peak of the Mg signal in Figure 5 reflects trends in the proxy record. The second largest peak of the Fourier spectrum is found at a frequency of one year^{-1} (assuming a constant growth rate of 4.8 mm year^{-1}). Several other peaks can be identified, viz. a peak at a frequency of approximately two year^{-1}, corresponding to variations with a six month period in the Mg signal are present; Even a third harmonic can be noticed. However, many other peaks in the spectrum remain unidentified and cause the weak correlation with SST.

4.3.1. TBD Method

[21] The TBD is isolated by applying the windowing and phase demodulation technique. The window covered the spectral contents from 0.57 year^{-1} to 1.43 year^{-1}, i.e., the region covered by the thick solid line in Figure 5. Besides the data record itself, the choice of this width is actually the only input demanded from the user. Figure 6 illustrates the influence of this choice: four plots of the TBD are shown with an increasing width of the window. Figures 6a and 6b do not show much variation in contrast to 6c and 6d. When

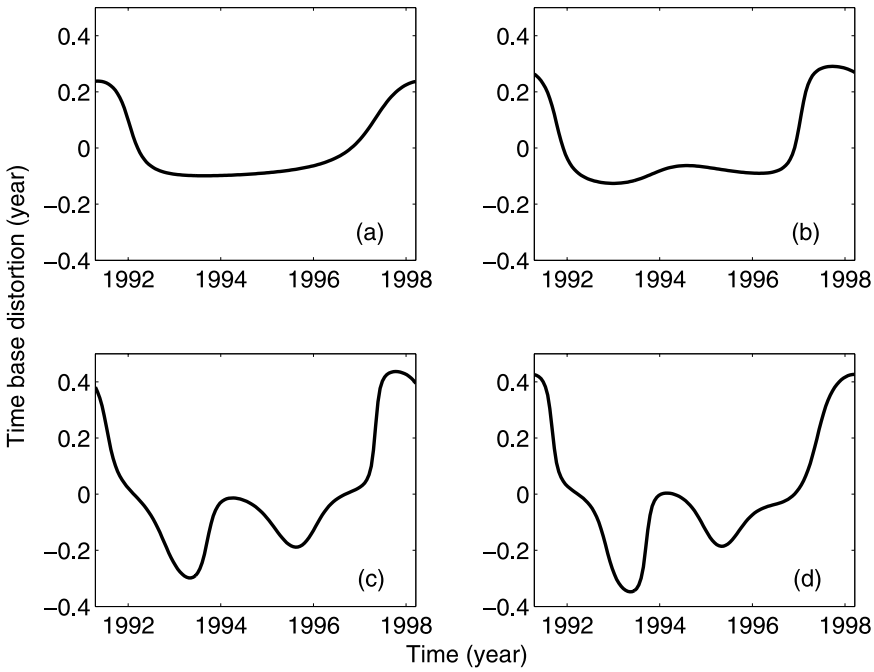

Figure 6. The TBD changes with increasing width of the window: (a) from 0.857 to 1.143 year^{-1}, (b) from 0.714 to 1.286 year^{-1}, (c) from 0.571 to 1.429 year^{-1}, and (d) from 0.429 to 1.571 year^{-1}. Notice that the beginning and end matched. This bias is due to the Gibbs phenomenon.

selecting the window width, the investigator should keep in mind that (1) by increasing the window width, the model errors, due to the bandwidth limitation, will decrease, (2) by decreasing the window width, the influence of stochastic noise decreases. Both aspects should be weighted. However, by increasing the window width to right, the possibility increases that the TBD around the second harmonic is erroneously included in the estimated TBD around the first harmonic; and a long-term trend, if present, appear at the left side of the first harmonic and may not be included in the window. To cope with long-term trends, we have detrended the record before estimating the TBD. Practically, it is our experience that a window width equal to the fundamental frequency performs well, because the model errors are minimized, while no overlap with the window around the second harmonic can occur.

4.3.2. Anchor Point Method

[22] It is assumed that the peaks in the Mg signal are annual and coincide with the peaks in the SST record. The peaks that we have selected are shown in Figure 4. Between two subsequent peaks a linear growth rate is assumed and the data before the first peak and after the last one are lost.

4.3.2.1. Reconstructed Growth Rate

[23] Using equation (2), an improved growth rate can be calculated. Figure 7 shows the growth rates

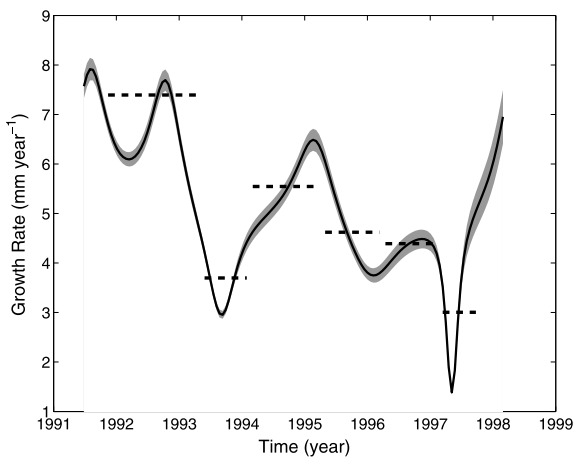

Figure 7. Growth rate of *I. ephippium* as function of the same time base as used in Figure 4: TBD (solid line) and anchor point method (dotted line). The gray area represents the 95% uncertainty bound estimated with a Monte Carlo simulation of 100 runs.

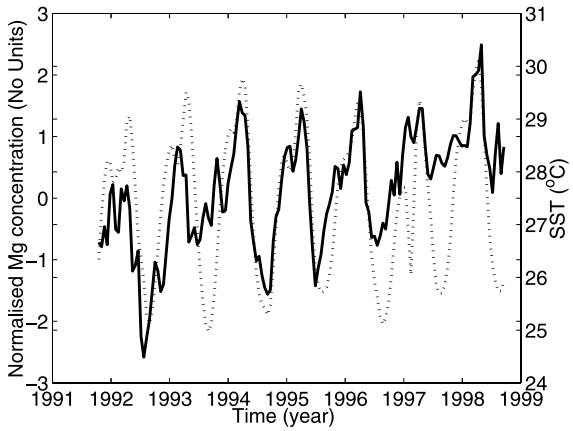

Figure 8. Mg signal (solid line) on the improved time grid compared with instrumental SST (dotted line).

calculated by both methods. Although the TBD method changes the time grid by only 5% (root-mean-square value of gT_s divided by the root-mean-square value of t, with g and t defined in equation (2)), the influence on the position of one single peak can be large. The TBD method provides a much more detailed profile of the variations in growth rate, but on the average, both follow the same trend, i.e., a decrease in growth rate, disturbed at two occasions. The most remarkable feature of the TBD growth rate is the detection of two large dips in growth rate (cooler seasons of 1993 and 1997). It is possible that growth rate stopped completely during these events, but this cannot be discerned because of the limited band width of the window, which filters out the high frequency components in the TBD.

4.3.2.2. Correlation With SST

[24] The discrete data points along the growth axis are no longer equidistant after correcting for growth rate variation. Therefore the measurements were resampled before comparing this Mg record with the SST. Employing the TBD method, a correlation coefficient R = 0.60 is found (between

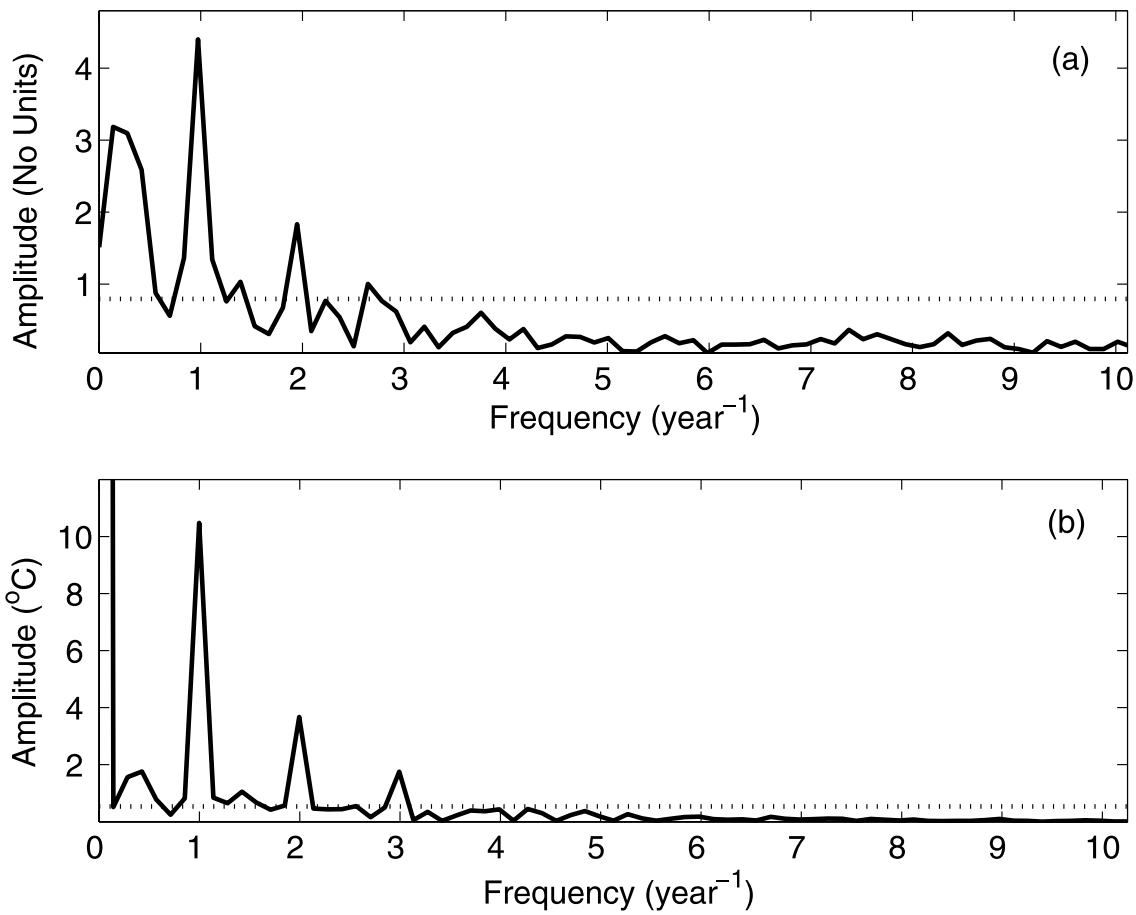

Figure 9. (a) Fourier spectrum of the Mg signal on the improved time grid; (b) Fourier spectrum of the instrumental SST. The dotted lines visualize the 95% uncertainty bounds.

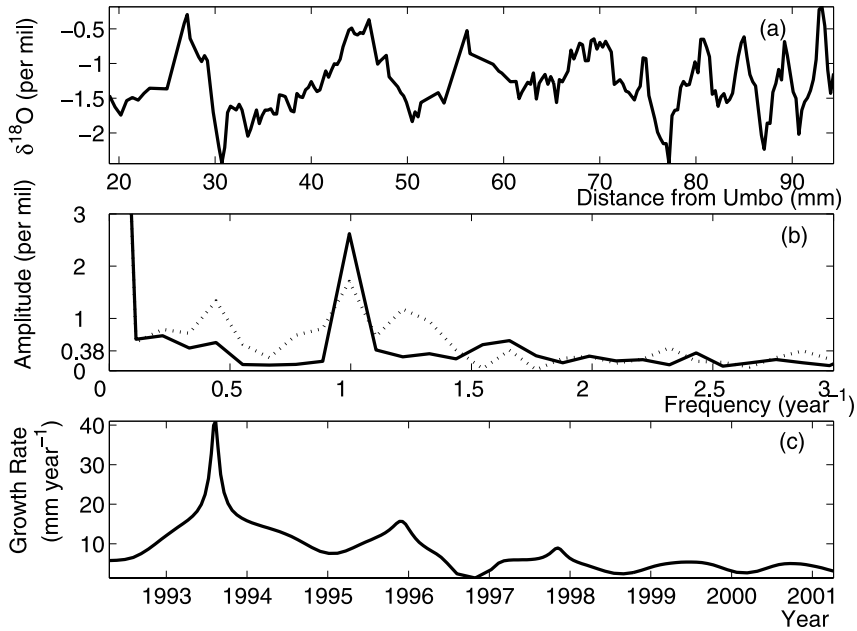

Figure 10. First *Saxidomus giganteus* from Washington State: (a) raw data, (b) Fourier spectra before (dotted line) and after (solid line) the TBD method (the 95% uncertainty bound is 0.38 per mil), and (c) growth rate (the mean 95% uncertainty bound estimated with a Monte Carlo simulation of 100 runs are at ±0.4 mm year^{-1}).

the normalized Mg and SST record), while the anchor point method yields a correlation coefficient of R = 0.57 (n = 145, both $p < 0.01$). Although the difference is small, for the TBD method it was not a priori necessary to assume that all maxima of the Mg record coincide with SST maxima. The anchor point method, on the contrary, a priori links Mg maxima to SST maxima.

[25] Figure 8 compares the resampled Mg data on the reconstructed time grid using the TBD method with the SST record. Note that nearly all yearly maxima and minima in both records correspond one to one. This is highlighted when taking a closer look at the Fourier spectra of both the Mg and the SST record (Figure 9):

[26] 1. The annual frequency in the Mg remains, as expected, but the amplitude is larger (compare the amplitude in Figure 5 with that in Figure 9a).

[27] 2. The peaks due to the TBD have disappeared and this not only around the first harmonic (which we used to calculate the TBD), but also around the second and third harmonic, although we have not used this information directly; this shows that the TBD acts identically on all harmonics as is expected from theory [*Verspecht*, 1994; *Schoukens et al.*, 1997]. This validates the initial assumptions that were made.

[28] 3. The second harmonic (biannual variations) stands out higher relative to the surrounding frequencies.

[29] 4. Even a third harmonic can be distinguished from the noise.

[30] 5. These three harmonics are also found in the spectrum of the SST.

[31] 6. The relative magnitude of the harmonics in the Mg signal and in the SST correspond as well, which indicates a static linear relation between both [*Pintelon and Schoukens*, 2001a].

[32] 7. The Mg record consists of a periodic signal, a trend and noise. The latter is now equally distributed over all frequencies, which means that the record is disturbed with white noise, probably due to measurement uncertainties. In order to visualize this, the 95% uncertainty bounds are calculated. Therefore the trend and the periodic signal were estimated and the uncertainty was estimated from the mismatch of these signals (assuming circular normally distributed white noise) [*Pintelon and Schoukens*, 1996, 2001b].

4.3.2.3. Trends in the Record

[33] There is no trend for SST but Mg clearly has one (Figure 8). This trend is isolated from the harmonics in the Fourier spectrum, and is

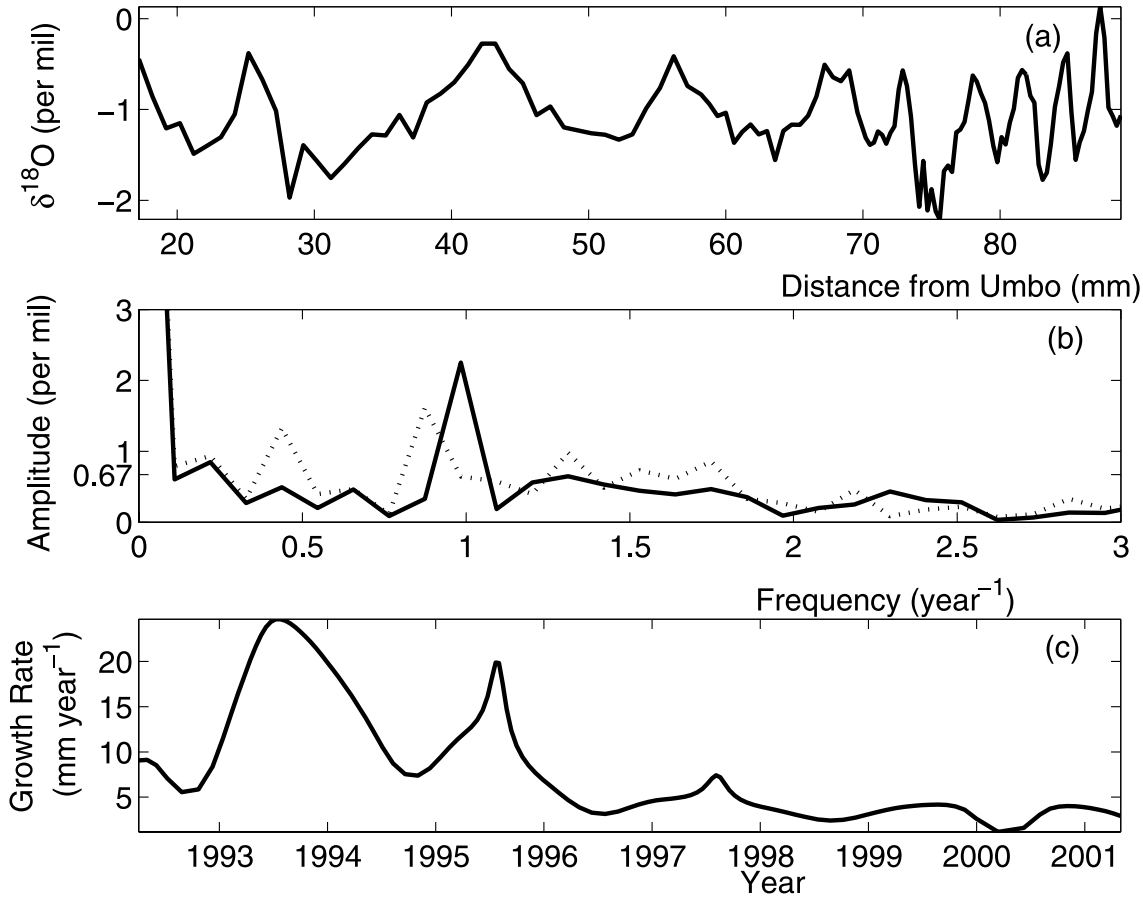

Figure 11. Second *Saxidomus giganteus* from Washington State: (a) raw data, (b) Fourier spectra before (dotted line) and after (solid line) the TBD method (the 95% uncertainty bound is 0.67 per mil), and (c) growth rate (the mean 95% uncertainty bound estimated with a Monte Carlo simulation of 100 runs are at ±0.3 mm year^{-1}).

expressed by the broad utmost left peak. A possible explanation is that an unknown process, additive to the SST, influences Mg (e.g., aging). When detrending the Mg record, the correlation with SST increases from R = 0.60 to R = 0.76. Thus most variation of the Mg proxy can be explained by SST and a long-term trend.

5. Case Study 2: *Saxidomus giganteus*

[34] In a second example the TBD method is illustrated on the stable oxygen isotope records (δ^{18}O) measured in the aragonite shells of *S. giganteus* from Puget Sound (Washington State, U.S.A.) in September 2001. For a detailed description of the experimental setup and interpretation of the results, we refer the interested reader to *Gillikin et al.* [2004]. This site generally experiences a SST range of 8°C (8°C to 16°C) and has a salinity of 27.7 ± 1.06‰, with occasional (less than yearly) periods of freshwater input reducing salinity to ca. 20‰. A thick-section of the aragonite shell was continuously sampled using a computer-controlled microdrill from growing tip to halfway to the umbo. The carbonate powder (±100 μg) was processed using an automated carbonate device (Kiel III) coupled to a Finnigan Delta+XL. Data were corrected using an internal laboratory standard and are reported relative to V-PDB in conventional notation. Precision is generally better than 0.08‰.

[35] Three different specimen were studied and the raw data are shown in Figures 10a, 11a, and 12a (see *Gillikin et al.* [2004] for more details). Since the specimens come from the same sampling site, we can expect that they have similarly recorded environmental conditions. The correlation between the records can thus be used to compare the anchor point method with the TBD method presented here. The three records consist of 190, 123 and 55 observations (for clam 1, 2 and 3 respectively;

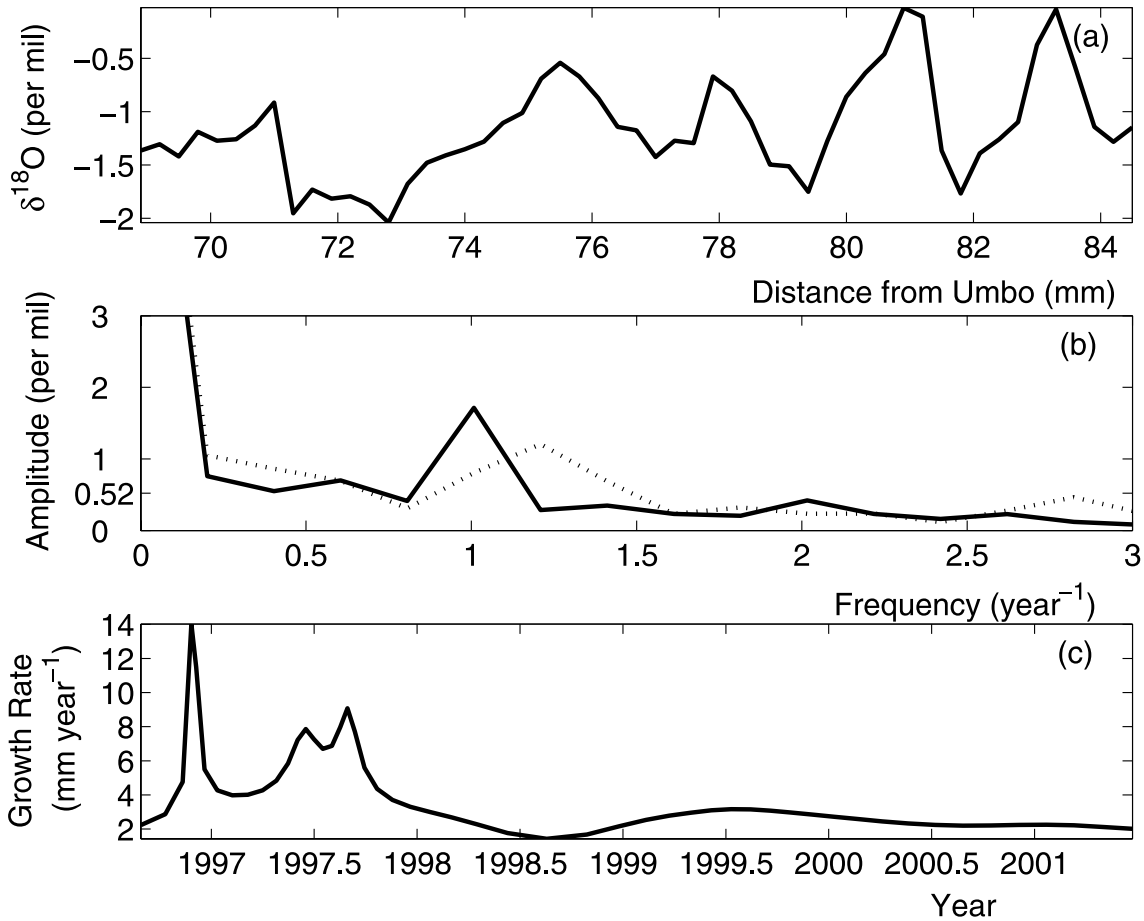

Figure 12. Third *Saxidomus giganteus* from Washington State: (a) raw data, (b) Fourier spectra before (dotted line) and after (solid line) the TBD method (the 95% uncertainty bound is 0.52 per mil), and (c) growth rate (the mean 95% uncertainty bound estimated with a Monte Carlo simulation of 100 runs are at ±0.3 mm year^{-1}).

clam 3 was not fully sampled) and covers periods of approximately five to nine years (assuming that periodic variations are annual). The dotted lines in Figures 10b, 11b, and 12b show the power spectra of the records, assuming constant growth rate. The full line shows the spectrum after correction for TBD, using a window covering the spectral contents from 0.762 to 1.238 year^{-1} (Clam 1), 0.628 to 1.372 year^{-1} (Clam 2) and 0.730 to 1.270 year^{-1} (Clam 3). Clearly, TBD correction leads to a simplification of the Fourier spectra: ghost peaks, hiding the growth rate information have now disappeared, while annual periodicity is highlighted. No other harmonics are significant in the spectra, which are shown by the 95% uncertainty bounds. These are estimated from the residual after a periodic signal was matched on the data (assuming circular normally distributed white noise) [*Pintelon and Schoukens*, 1996, 2001b]. The three δ^{18}O records on the TBD corrected time bases are shown in Figure 13. Similar features can be found in all records, such as the broad relatively high minimum during summer 1998 and the much more negative values in summer 1997. These similarities are reflected by the high correlation coefficients between the three series (Table 2). In order to calculate these correlation coefficients the observations were interpolated on the time axis of clam 2. Using the correlation between the records as criterion, the time base estimated with the TBD method is in all cases slightly better then the one calculated with the anchor point method. The reason for this is that the anchor point method fixes the annual minima, while the phase demodulation restores the periodic component at all observations. Clearly, the TBD method outperforms the anchor point method.

[36] In Figures 10c, 11c, and 12c, the growth rates of the samples are shown. The TBD method can give a more refined growth rate profiles. Similar trends can be detected in the growth rate profiles in all three specimens: on average, growth rate

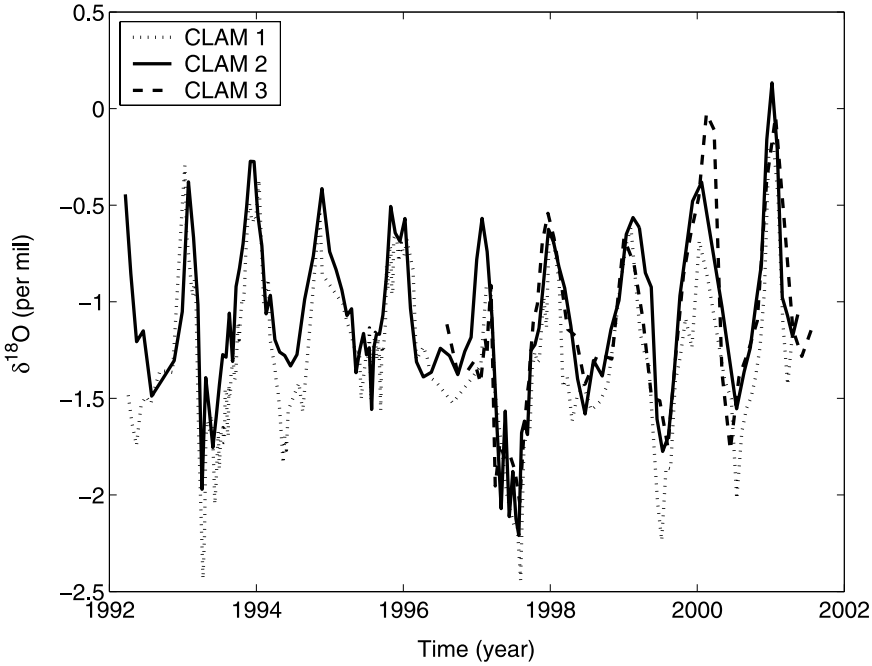

Figure 13. The three $\delta^{18}O$ signals as function of the time, which was estimated by the phase demodulation method.

decreases with time, while in between 1997 and 1998 growth rate was high for the three clams, while it was low in late 1996 and early 2000 for clam 1 and 2. Again we emphasize that the width of the window limits the variations in growth that can be detected by this method. This means that detailed variation on subannual scale is out of reach in this example. To solve this problem, parametric growth rate models can be used [*Schoukens et al.*, 1997].

6. Case Study 3: Vanuata Coral Stable Isotope Record

[37] In this section we illustrate how the TBD method can be used as a refinement of an existing time base and how an unknown frequency on a distorted time base can be identified. Therefore we processed the Vanuatu coral $\delta^{18}O$ record, covering a period of 173 years, published by *Quinn et al.* [1996] (additional information about the instrumentation and the data can be downloaded from http://www.ngdc.noaa.gov/paleo/). Ages were originally derived from annual density banding, combined with the anchor point method. This procedure may introduce nonnegligible errors in the time base, as we showed earlier for the simulation (section 3). Assuming now that the record is periodic, the TBD, $g(n)$, can be calculated and the timing of each observation can be refined.

[38] The data record is shown in Figure 14a, and its spectrum is shown in Figure 14b. Notice that the spectral information is spread along the frequencies 0.05 to 0.10 year^{-1}, which makes the identification of the underlying 14–15 year periodicity a difficult task. In this case study, we do not know in advance the distorted frequency around which the TBD can be estimated. Figure 14b shows several neighboring peaks and it is unclear which are caused by variations in accretion rate or by the hidden periodic variation in the record. To overcome this problem, the TBD was initially estimated around the largest peak in the region of interest (0.075 year^{-1}) using a window covering the spectral contents from 0.046 year^{-1} to 0.104 year^{-1}. As shown in Appendix B, an incorrect initial estimate

Table 2. Correlation Coefficients, R, Between the Three *Saxidomus giganteus* Stable Isotope Records Sampled at the Same Site in Washington State

	Correlation, R		
	1 Versus 2	1 Versus 3	2 Versus 3
TBD	0.91	0.90	0.88
Anchor Point	0.81	0.79	0.85

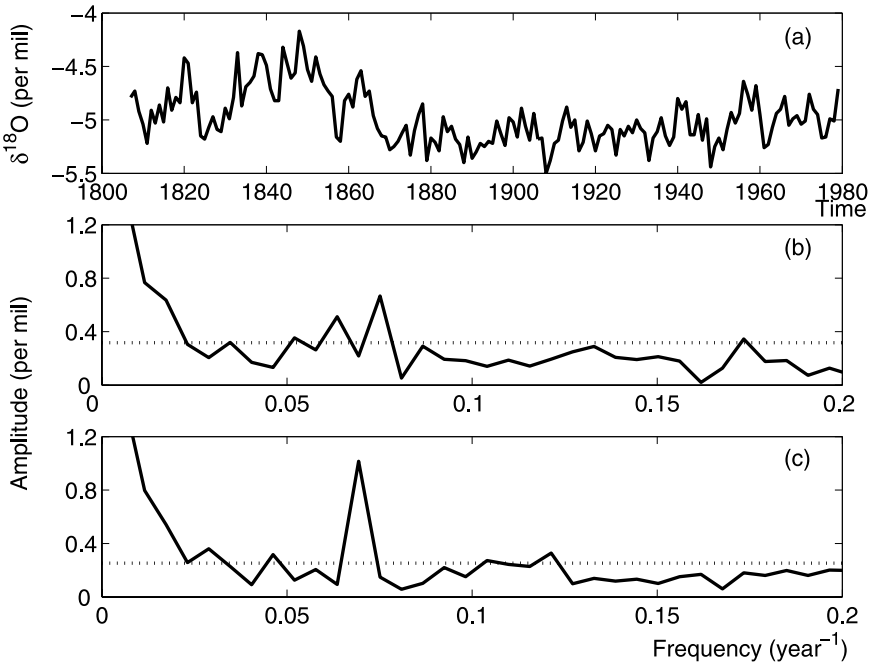

Figure 14. (a) The measured $\delta^{18}O$ signal of the coral in the time domain (before TBD correction); (b) the corresponding Fourier spectrum; (c) Fourier spectrum of the time base corrected growth rate. The dotted lines visualize the 95% uncertainty bounds.

of the frequency will cause a linear trend in the TBD. The slope of this linear trend is proportional to the mismatch between the initially estimated frequency and the "true" frequency. An iterative procedure is used to refine the frequency estimate until the optimal frequency is found (corresponding to a slope of zero). The Fourier spectrum corresponding to the improved time base is shown in Figure 14c: the record can be decomposed in a trend (the broad peak left in the spectrum) and one single peak with a frequency of 0.0693 year^{-1} (i.e., a periodicity of 14.42 years). To validate the improvements made, the original and the TBD time base were first detrended (sixth order polynomial). Next a periodic signal was matched to the remaining signal [*Pintelon and Schoukens*, 1996] and the uncertainty was estimated from the mismatch of these signals (assuming circular normally distributed white noise). This is visualized by the 95% uncertainty bound on the spectra [*Pintelon and Schoukens*, 2001b]. Refining the time base increases the signal-to-noise-ratio on the harmonic from 4.2 to 8.2. To conclude, assuming that a periodic component with a frequency in the region 0.05 to 0.10 year^{-1} is present in the record, the TBD is useful to refine the initially estimated time base. This leads to the identification of a single harmonic with a frequency of 0.0693 year^{-1} (i.e., occurring at a periodicity of 14.42 years), which simplifies the spectral interpretation quite a lot.

7. Conclusion

[39] We have presented a new method to reconstruct changes in the growth/accretion rate of proxy environmental records, based on the periodic content of proxy series. This approach is useful for a better reconstruction of the time series. The two weak points of this method are the constraints (1) that the record has to have a periodic component and (2) that the bandwidth of the TBD is limited. The main benefit is that it can reconstruct variations in growth or accretion rates, including short growth or accretion stops, in much more detail than the anchor point method.

[40] Both methods were first compared using synthetic data. Next they were applied to the Mg record in a bivalve, *I. ephippium*, from Kenya, where the Mg record could be correlated with SST. In this example the benefits and limitations of both methods are illustrated. Next, three specimens of the clam *Saxidomus giganteus* sampled from the same site are processed and discussed. In this case the correlation between the three records along the estimated time bases is used to illustrate the better perfor-

mance of the TBD method compared to the anchor point method. Finally, the TBD approach applied on the Vanuatu coral stable isotope record dated, using growth bands and the anchor point method. In this last case study, we have illustrated that the TBD method can also be applied to refine the time base estimated with the anchor point method. Our TBD approach performed well on a simulation, as well as on five real world examples. Interpretation of other proxy records could also benefit form this approach that enables to reconstruct a more detailed time base.

Appendix A

[41] The mathematical framework was first proposed by *Verspecht* [1994] and worked out in more detail by *Schoukens et al.* [1997]. The Fourier spectrum, S, of the record, s, can be calculated using a discrete Fourier transformation algorithm (DFT):

$$S(\omega) = \mathrm{DFT}[s(t)]. \tag{A1}$$

The TBD is isolated by windowing the spectrum, $S(\omega)$, with a rectangular window, $c(\omega)$, around the first harmonic. This cuts out an estimate, $\hat{G}(\omega)$, of the spectrum (for example, an estimate of the shifted spectrum $\hat{G}$ could be the left triangle in Figure 2b):

$$G(\omega) = c(\omega)S(\omega), \tag{A2}$$

with $c(\omega) = 1$ if ω is in the frequency range of interest (for example $\omega_0 - b < \omega < \omega_0 + b$, with b half the width of the window) and $c(\omega) = 0$ elsewhere. The calculation of an estimate of the TBD, $\hat{g}(n)$, is completed by employing the inverse discrete Fourier transformation (IDFT):

$$\hat{g}(n) = \frac{\varphi\left[\exp(-j(\omega_0/\omega_s)2\pi n)\mathrm{IDFT}\left(\hat{G}\right)\right]}{\omega_0}, \tag{A3}$$

with $\varphi(u)$ the phase of u, $j = \sqrt{-1}$, ω_0 the fundamental radial frequency (2π/age (year^{-1})) and ω_s the radial sampling frequency $2\pi/T_s$, with T_s the sample period (average time gap between two subsequent observations). The exponential term shifts the frequency by $-\omega_0$.

Appendix B

[42] The argument of the Fourier series of the record is given by

$$\omega(nT_s + g(n)T_s), \tag{B1}$$

where ω is the fundamental frequency, n is the observation number, T_s is the sample period and $g(n)$ is the TBD at observation n. If the fundamental frequency, around which the TBD manifests, is initially incorrectly estimated, this estimated frequency, $\hat{\omega}$, can be written as a scaled actual frequency, ω,

$$\hat{\omega} = (1 + \alpha)\omega, \tag{B2}$$

where α is the relative frequency error ($\alpha < 0$ means an underestimation of the fundamental frequency and thus an underestimation of the actual age of the specimen; $\alpha = 0$ means a good estimation and $\alpha > 0$ means an overestimation and thus an overestimation of the actual age). Equation (B2) is now inserted into equation (B1) in order to express the TBD as a linear trend additive to another TBD,

$$\begin{aligned}\hat{\omega}[nT_s + h(n)T_s] &= \omega[1 + \alpha][nT_s + h(n)T_s] \\ &= \omega[nT_s + \alpha nT_s + (1 + \alpha)h(n)T_s] \\ &= \omega[nT_s + g(n)T_s],\end{aligned} \tag{B3}$$

from which it follows that

$$g(n) = [1 + \alpha]h(n) + \alpha n, \tag{B4}$$

where $h(n)$ is related to $g(n)$ as equation (B4) shows that a misidentification of the fundamental frequency ($\hat{\omega}$ instead of ω) leads to a linear trend (αn) in the TBD, $g(n)$. In the latter case the value of α can be used to adapt the improved estimation of the fundamental frequency.

Acknowledgments

[43] We thank Jelle Bijma (Pelagic Ecosystems - Marine Carbon Fluxes; Geowissenschaften, Bremen, Germany) for a helpful discussion and comments on this manuscript. Claire Lazareth kindly provided LA-ICP-MS data from the *I. ephippium*. This work is sponsored by the Fund for Scientific Research (FWO-Vlaanderen), the Flemish Government (GOA-IMMI) and the Belgian Program on Interuniversity Poles of Attraction initiated by the Belgian State, Prime Minister's Office, Science Policy programming (IUAP 5) and the Federal Science Policy Office PODO II Programme on Global Change and Biodiversity, Brussels, Belgium (Contract EV/03/04B).

References

Fallon, S. J., M. T. McCulloch, R. van Woesik, and D. J. Sinclair (1999), Corals at their latitudinal limits: Laser ablation trace element systematics in porites from Shirigai Bay, Japan, *Earth Planet. Sci. Lett.*, *172*, 221–238.

Finch, A. A., P. A. Shaw, G. P. Weedon, and K. Holmgren (2001), Trace element variation in speleothem aragonite: Potential for palaeoenvironmental reconstruction, *Earth Planet. Sci. Lett.*, *186*, 255–267.

Gillikin, D. P., H. Ulens, F. De Ridder, M. Elskens, E. Keppens, W. Baeyens, and F. Dehairs (2004), Assessing the reproducibility and reliability of estuarine bivalve shells (*Saxidomus giganteus*) for sea surface temperature reconstruction: Implications for paleoclimate studies, *Palaeogeogr. Palaeoclimatol. Palaeoecol.*, in press.

Herbert, T. D. (1994), Reading orbital signals distorted by sedimentation: Models and examples, in *Orbital Forcing and Cyclic Sequences*, edited by P. L. deBoer and D. G. Smith, *Spec. Publ. Int. Assoc. Sedimentol.*, *19*, 483–507.

Jones, D. S. (1983), Sclerochronology: Reading the record of the molluscan shell, *Am. Sci.*, *71*, 384–390.

Klein, R. T., K. C. Lohmann, and C. W. Thayer (1996), Bivalve skeletons record sea-surface temperature and $\delta^{18}O$ via Mg/Ca and $^{18}O/^{16}O$ ratios, *Geology*, *24*(5), 415–418.

Kuhnert, H., J. Patzold, B. Schnetger, and G. Wefer (2002), Sea-surface temperature variability in the 16th century at Bermuda inferred from coral records, *Palaeogeogr. Palaeoclimatol. Palaeoecol.*, *179*, 159–171.

Lazareth, C. E., P. Willenz, I. Navez, E. Keppens, F. Dehairs, and L. André (2000), Sclerosponges as a new potential recorder of environmental changes: Lead in *Ceratoporella nicholsoni*, *Geology*, *28*, 515–518.

Lazareth, C. E., E. Vander Putten, L. André, and F. Dehairs (2003), High-resolution trace element profiles in shells of the mangrove bivalve *Isognomon ephippium*: A record of environmental spatio-temporal variations?, *Estuarine Coastal Shelf Sci.*, *56*, 1–12.

Marshall, J. F., and M. T. McCulloch (2002), An assessment of the Sr/Ca ratio in shallow water hermatypic corals as a proxy for sea surface temperature, *Geochim. Cosmochim. Acta*, *66*, 3263–3280.

Martinson, D. G., N. G. Pisias, J. D. Hays, J. Imbrie, T. C. Moore, and N. J. Shackleton (1987), Age dating and the orbital theory of the ice age: Development of a high resolution 0 to 300000–year chronostratigraphy, *Quat. Res.*, *27*, 1–29.

Paillard, D., L. Labeyrie, and P. Yiou (1996), Macintosh program performs time-series analysis, *Eos Trans. AGU*, *77*(39), 379.

Petit, J., et al. (1999), 420,000 years of climate and atmospheric history revealed by the Vostok deep Antarctic ice core, *Nature*, *399*, 429–436.

Pintelon, R., and J. Schoukens (1996), An improved sine-wave fitting procedure for characterizing data acquisition channels, *IEEE Trans. Instrum. Meas.*, *45*(2), 588–593.

Pintelon, R., and J. Schoukens (2001a), *System Identification: A Frequency Domain Approach*, IEEE Press, New York.

Pintelon, R., and J. Schoukens (2001b), Measurement of frequency response functions using periodic excitations, corrupted by correlated input/output errors, *IEEE Trans. Instrum. Meas.*, *50*(6), 1753–1760.

Quinn, T. M., T. J. Crowley, and F. W. Taylor (1996), New stable isotope results from a 173-year coral record from Espiritu Santo, Vanuatu, *Geophys. Res. Lett.*, *23*(23), 3413–3416.

Schoukens, J., R. Pintelon, and G. Vandersteen (1997), A sinewave fitting procedure for characterizing data acquisition channels in the presence of time base distortions and time jitter, *IEEE Trans. Instrum. Meas.*, *40*(4), 1005–1010.

Sinclair, D. J., L. P. J. Kinsley, and M. T. McCulloch (1998), High resolution analysis of trace elements in corals by laser ablation ICP-MS, *Geochim. Cosmochim. Acta*, *62*(11), 1889–1901.

Vander Putten, E., F. Dehairs, L. André, and W. Baeyens (1999), Quantitative in situ microanalysis of minor and trace elements in biogenic calcite using infrared laser ablation–inductively coupled plasma mass spectrometry: A critical evaluation, *Anal. Chim. Acta*, *378*, 261–272.

Vander Putten, E., F. Dehairs, E. Keppens, and W. Baeyens (2000), High resolution distribution of trace elements in the calcite shell layer of modern *Mytilus edulis*: Environmental and biological controls, *Geochim. Cosmochim. Acta*, *64*(6), 997–1011.

Verheyden, S., E. Keppens, I. J. Fairchild, F. McDermott, and M. Weis (2000), Mg, Sr and Sr isotope geochemistry of a Belgian Holocene speleothem: Implications for palaeoclimatic reconstructions, *Chem. Geol.*, *169*, 144–161.

Verspecht, J. (1994), Accurate spectral estimation based on measurements with a distorted-timebase digitizer, *IEEE Trans. Instrum. Meas.*, *43*(2), 210–215.

Weedon, G. P. (1989), The detection and illustration of regular sedimentary cycles using Walsh power spectra and filtering, with examples from the Lias of Switzerland, *J. Geol. Soc.*, *146*, 133–144.

Wei, G., M. Sun, X. Li, and B. Nie (2000), Mg/Ca, Sr/Ca and U/Ca ratios of a porities coral from Sanya Bay, Hainan Island, South China Sea and their relationship to sea surface temperature, *Palaeogeogr. Palaeoclimatol. Palaeoecol.*, *162*, 59–74.